THERMAL ANALYSIS OF THE CYLINDER BLOCK OF AN AXIAL PISTON PUMP – THE KEY TO MONITORING EFFICIENCY

Roman Ivantysyn*, Jürgen Weber, Alexander Kunze, Wieland Uffrecht

Institute of Mechatronic Engineering, Technische Universität Dresden, Helmholtzstrasse 7a, 01069 Dresden

* Corresponding author: Tel.: +49 351 463-33701; E-mail address: roman.ivantysyn@tu-dresden.de

ABSTRACT

To prepare today's fluid power systems for the future digitalization of the industry, it is necessary to improve the information available regarding the current condition of crucial components of the system. Positive displacement machines, which constitute the core of any hydraulic system, play a vital role in this process. Future smart systems will require more information about the current state of the pump such as power usage and efficiency. Current condition monitoring approaches utilize an array of sensors that need to be sampled at high frequency. The transmission, storage, and post processing of this vast amount of data requires an enormous number of resources, especially if exercised at scale. Previous work conducted at the Institute of Mechatronics Engineering at TU Dresden has demonstrated that measuring the temperature in the lubricating gaps can allow for a deeper insight into the tribological mechanisms in these interfaces. Not only can the gap height, viscous friction and leakage be determined from this information, but also crucial information such as wear level and expected component lifespan can be derived from temperature levels with adequate reference models [1]–[4]

This paper demonstrates that monitoring the thermal condition of the cylinder block is an effective approach to estimate the pump's efficiency. This will be illustrated through both simulation and measurement, in addition to the pioneering measurement of the heat convection coefficient on the cylinder block surface, a critical boundary condition for the simulation.

To measure the temperature of a moving cylinder block, a 160cc axial piston pump was equipped with a telemetric system, which was specially designed and built for this task. Next to the 20 temperature sensors four heat convection coefficient sensors were also carefully placed inside the cylinder block. The resulting measurements did not only validate the simulation but also give a unique insight into the inner workings of a piston pump.

Keywords: Temperature, efficiency, axial piston pump

1. MOTIVATION

The prevailing methodology for condition monitoring relies on a black-box strategy. This method predominantly employs sensors to observe pressure or vibration signals in the frequency domain. Subsequently, this data undergoes processing through artificial intelligence mechanisms to forecast potential breakdowns. While this approach has shown promise, it is contingent on the availability of extensive data sets, which are not universally attainable. The applicability of this data-driven approach is constrained by factors such as the specific manufacturer, operating conditions, user practices, maintenance routines, and the type of hydraulic oil employed. Consequently, this approach remains largely accessible only to the largest corporations capable of amassing substantial datasets, and even for them, it may not be suitable for all pump types and sizes. Moreover, unlike consumer products like automobiles, axial piston pumps are not ubiquitous. This limits the pool of data crucial

for predictive maintenance strategies, further complicating the pursuit of data-intensive predictive maintenance methods.

In light of these limitations, this paper seeks to introduce a novel approach to condition monitoring centered on temperature measurements. Temperature is a readily measurable parameter that can be effortlessly recorded and stored, demanding only minimal bandwidth for data transmission. Within the thermal field of an axial piston pump lies a wealth of information, encapsulating the complex interplay between viscous losses that produce heat and volumetric losses that disperse heat via leakage.

The primary objective of this paper is to demonstrate the existence of a direct correlation between a pump's efficiency, characterized by its losses, and its temperature. To illustrate this relationship, the focus was set on the temperature field of the cylinder block of a 160cc open circuit pump. A cross section of the pump along with the simulated temperature field and the measured correlation between hydromechanics efficiency with its temperature level is shown in **Figure 1**. This paper shows how to simulate this trend accurately and how the measurements were performed. With capabilities to accurately forecast a pump's temperature field, a digital twin can not only deduce the pump's current state but also, given sufficient training data, anticipate looming failures. Beyond merely predicting failures, this method offers invaluable insights into the axial piston machine's current efficiency.

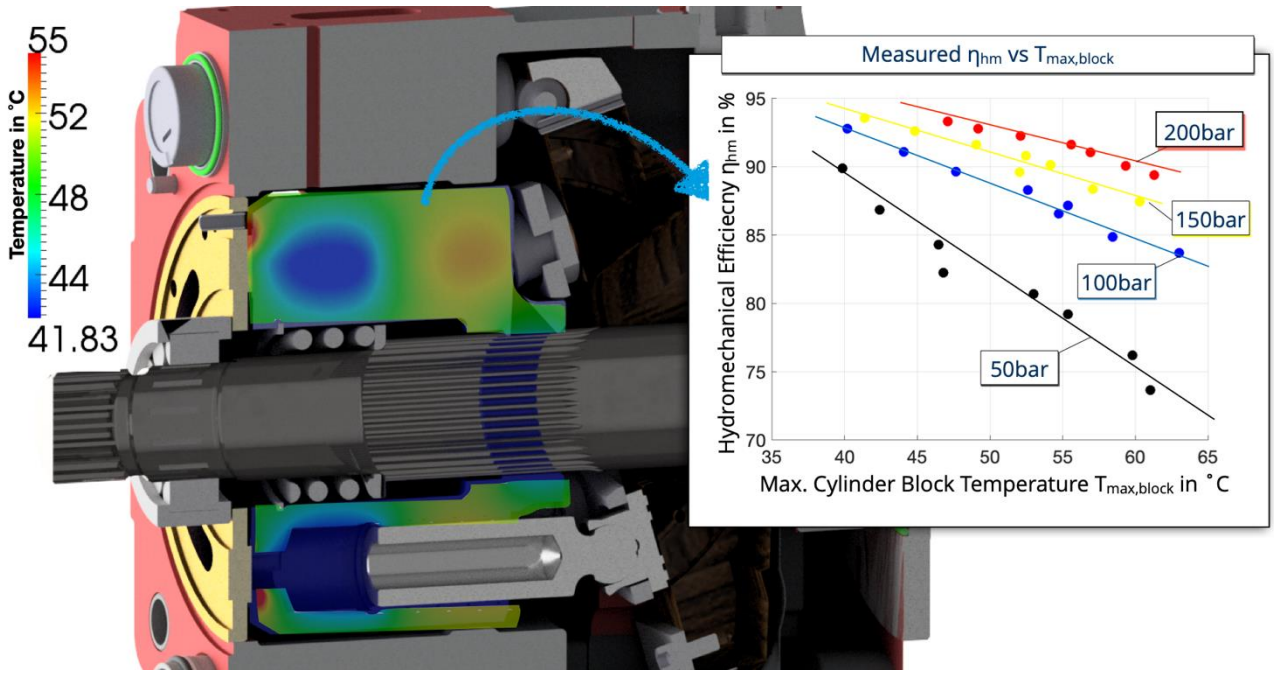

Figure 1: 160cc pump rotating kit, expected temperature field and measured hydromechanic efficiency trend with maximum cylinder block temperature.

2. RESEARCH GOAL AND APPROACH

The primary aim of this research is to devise a methodology to monitor the efficiency of an axial piston pump through the evaluation of the cylinder block's surface temperature. To achieve this goal the following steps are required:

1. Build a comprehensive model of the entire pump in Caspar FSTI to establish the relationship between temperature and efficiency.
2. Validate the model by conducting a pump efficiency test on an unaltered version.

3. Adapt the pump to facilitate thermal evaluations of the rotating cylinder block without altering its efficiency-influencing gap behavior.
4. Highlight prominent thermal facets from the measurements, offering potential industrial benefits.
5. Refine the pump model boundaries based on these measurements.
6. Propose a viable strategy to monitor hydrostatic pump efficiency.

The simulation model was built using Caspar FSTI and serves as a predictive tool, enabling the estimation of losses within all three lubricating gaps of the pump. The ability to simulate the pump's temperature field and efficiency is crucial, given the impracticality of such detailed measurements in industrial settings. This digital twin can serve both as a reference point to ideal conditions and nominal part dimensions and as a comparative tool to gauge efficiency, lifetime and wear-in.

To validate the tool, reference measurements of the pump's efficiency were conducted before any modifications were introduced to the pump. These reference measurements served as a benchmark against which the simulation results were compared. These measurements furnished a comparative framework to ascertain the simulation model's predictive accuracy in terms of efficiency and ensured that any modifications did not adversely impact the pump's performance.

After the validation the pump was modified, including the strategic placement of temperature sensors at locations determined through simulated temperature field analysis. These sensors captured even nuanced temperature gradients across the cylinder block, revealing its thermal dynamics during operation. Coupled FEM analysis, which used the piston load from the gap simulation, were used to estimate the blocks lifetime with various sensor configurations. As part of this task a novel telemetric system was deployed, which was developed by Dr. Uffrecht for high bandwidth measurements in a high speed rotational environment. It was previously used for temperature and pressure measurements in turbine applications [12]–[14].

To enhance the fidelity of the simulation model the measurements will be used to improve the thermal boundary conditions. For the gap simulations it is necessary to estimate the temperature surrounding the pump parts as well as the heat convection coefficients. Conventionally, these heat convection coefficients are estimated using analytical equations for simplified geometries or CFD simulations, as was also done for this pump. Given the inherent variability in literature-based values, there was a compelling need to measure these coefficients directly. A pioneering sensor, previously developed but untested in oil-based applications, was mobilized for this purpose [14]–[17]. This groundbreaking approach not only improves the precision of the gap simulation but also serves as a validation mechanism for the CFD simulations conducted throughout the study.

3. LITERATURE

In the past numerous researchers focused on the thermal analysis as well as the study of the lubricating gaps in hydrostatic machines. The first comprehensive thermal investigations that linked temperature with efficiency have been published by Schlösser and Witt in 1976 [18], [19]. In their studies the stationary thermal behavior of the fluid line temperature was successfully linked with the efficiency of pumps and motors. The concept was confirmed both in theory, using entropy and enthalpy terms, and measurement. The practicality of their findings is lacking the time aspect, e.g. the amount of time it takes for the line temperatures to reach steady state conditions and the distinction of where these losses occur, but nevertheless pave the way for a comprehensive thermal – efficiency model.

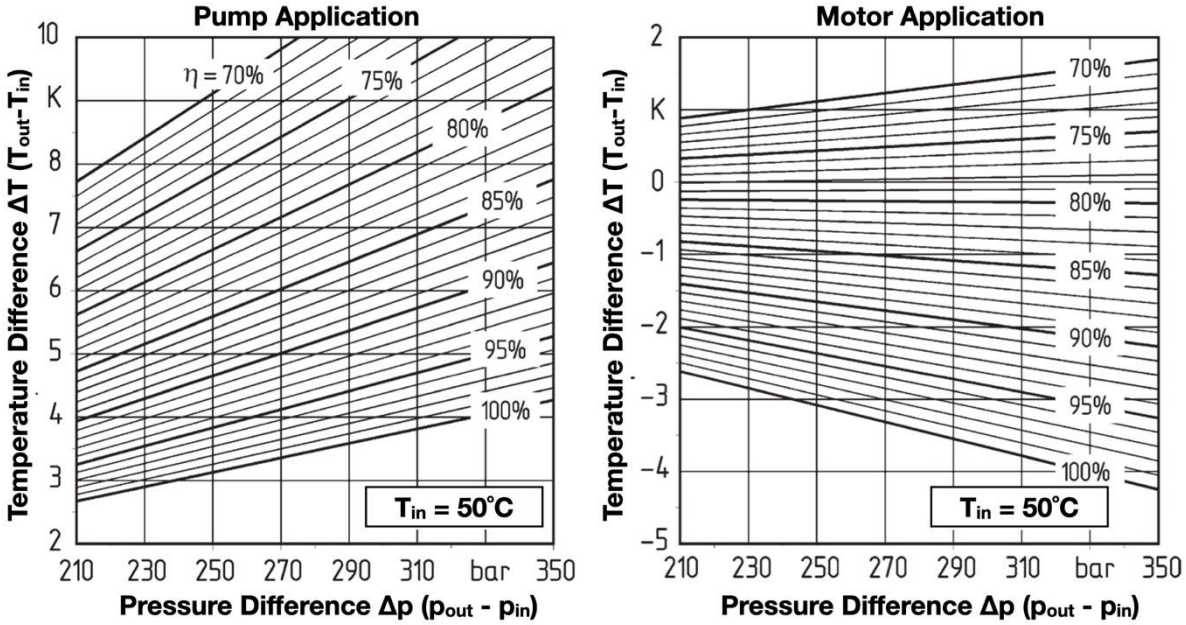

Figure 2: Total efficiency of the hydrostatic machine at steady state line conditions [20]

To understand where these losses occur and under what conditions, a gap analysis is necessary. In the era preceding advanced computational modeling, the fluid gaps of these machines were studied empirically, mostly with highly modified pump components on specialized test rigs. The body of scholars contributing to this domain is vast, hence only a short overview will be given. Test rigs that analyzed the micro movement and pressure distribution gave insight on the necessary gap heights, surface finish and analytical design methods [21]–[28]. As most of these empirical studies were not performed in an actual pump environment, efficiency tests were infeasible. In the past two decades sensors and electronics have allowed for a less invasive measurement of both gap height and temperature in fully functional pumps [9]–[11], [24], [25], [29]–[32]. However, the findings mostly focused on the validation of simulation models, rather than a pump analysis. Most investigations were confined to a singular lubricating gap, missing a holistic analysis of the pump.
In an effort to tackle this problem the author has built a test rig where two out of the three lubricating gaps were monitored both in gap height and temperature [1], [5], [33]. The work gave a unique insight into the thermal conditions in a pump over its entire working regime, demonstrating the unique behavior of each gap, as shown in **Figure 3**.

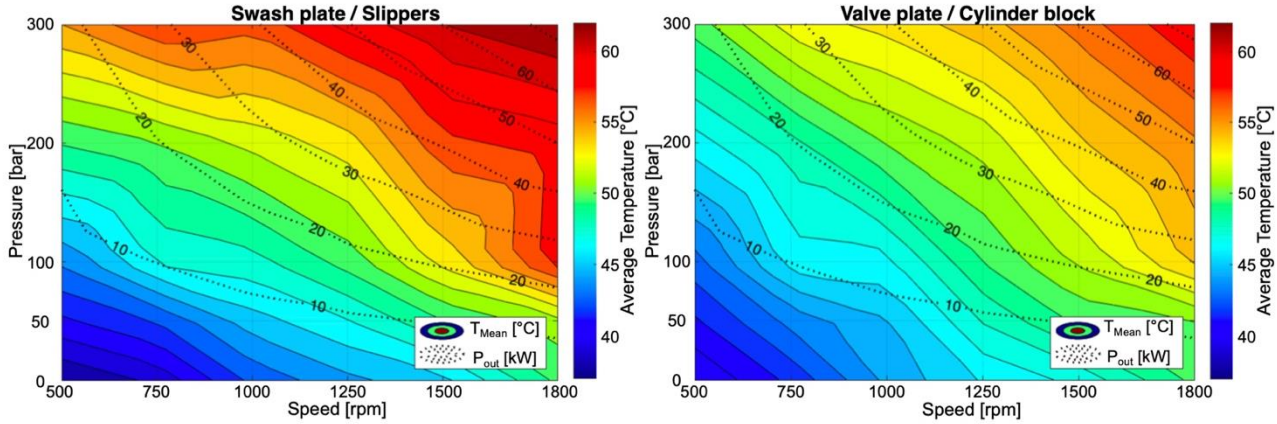

Figure 3: Simultaneous temperature measurements at both valve plate and swash plate [1]

The findings also showed that there is a direct correlation between temperature in the gap and its power loss, which was derived from the measured gap heights (see **Figure 4**). While the trend between

the piston and the cylinder block was captured exclusively in simulation, it mirrored parallel trends, e.g., an apparent pattern across varying pressure levels. This research endeavors to integrate the final missing link: the measurement of the cylinder block's temperature. In doing so, it paves the way for an exhaustive thermo-energetic dissection of the lubricating gaps.

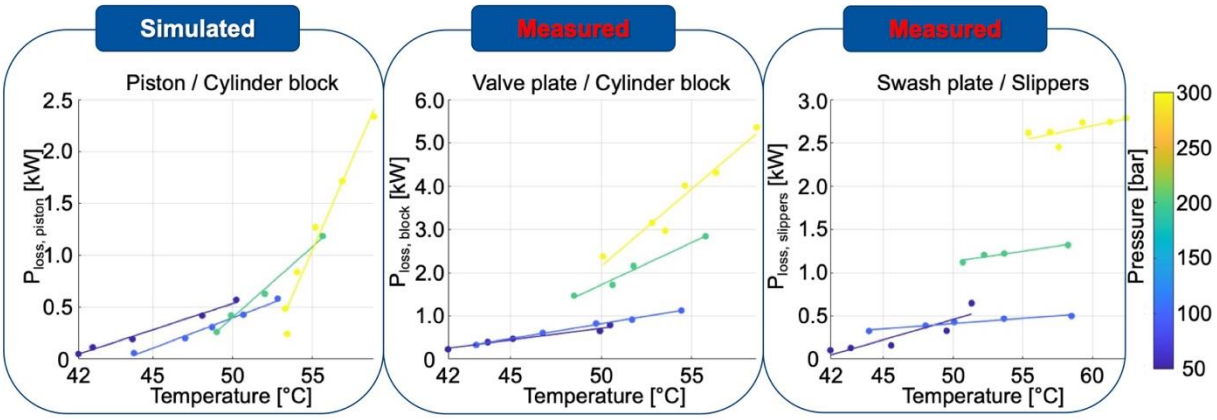

Figure 4: Predicted power loss vs temperature at all three lubricating gaps [1]

4. SIMULATION PREDICTION

Building on the gained knowledge presented in [1], where an entire pump model was built for a 92 cc open circuit pump and compared to measurements both in temperature, gap height and efficiency, a larger 160cc pump from Inline Hydraulics was chosen. This pump was not only used to simulate and validate the piston/cylinder gap simulation model, but also to confirm that the proclaimed temperature-efficiency trends are universally applicable.

4.1. Utilizing Caspar FSTI for advanced axial piston machine simulation

The modelling approach of Caspar FSTI is extensively detailed in [9]–[11], [34]. The credibility of the simulation model is fortified by extensive measurements of gap heights and temperature profiles, independently verified by Schenk [10] and Ivantysyn [5] for the slipper, and temperature measurements for the valve plate by Zecchi [11] and Ivantysyn [2]. The piston/bushing interface was validated using temperature measurements by Pelosi [9], however these measurements were performed for a highly modified singular and stationary bushing, instead of a moving cylinder block. All studies exhibited remarkable agreement between simulation and measurement, instilling high confidence in Caspar FSTI.

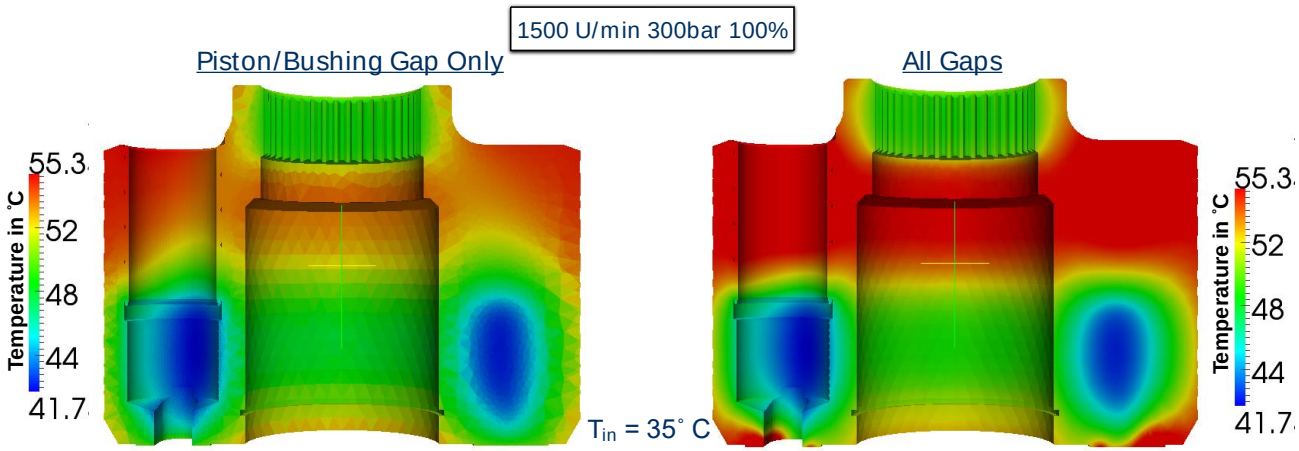

Figure 5: Cylinder block temperature due to piston gap only (left) and considering all 3 gaps (right).

In this study, a 160cc axial piston pump was modelled in simulation for all three main lubricating gaps. Even though the main focus is the cylinder block, a complete pump model is necessary in order to capture all cross interactions and the overall pumps efficiency. The strong influence of the gaps performance on the temperature field of the block is demonstrated in **Figure 5**, where the temperature field is shown with just the piston/bushing gap active (left) and with both other gaps simulated on the right, underlining the necessity to simulate all gaps when trying to accurately predict the block temperature.

Caspar FSTI's capabilities extend to solving the pressure field, temperature field, and micro motion of the entire rotating kit, considering thermal and pressure-induced deformations. This integrated approach yields invaluable data, but more importantly enables the prediction of the power losses in the individual interfaces and the entire pump. The power losses for an example operating point for the 160cc pump are shown in **Figure 6** split up into slipper, valve plate and block losses.

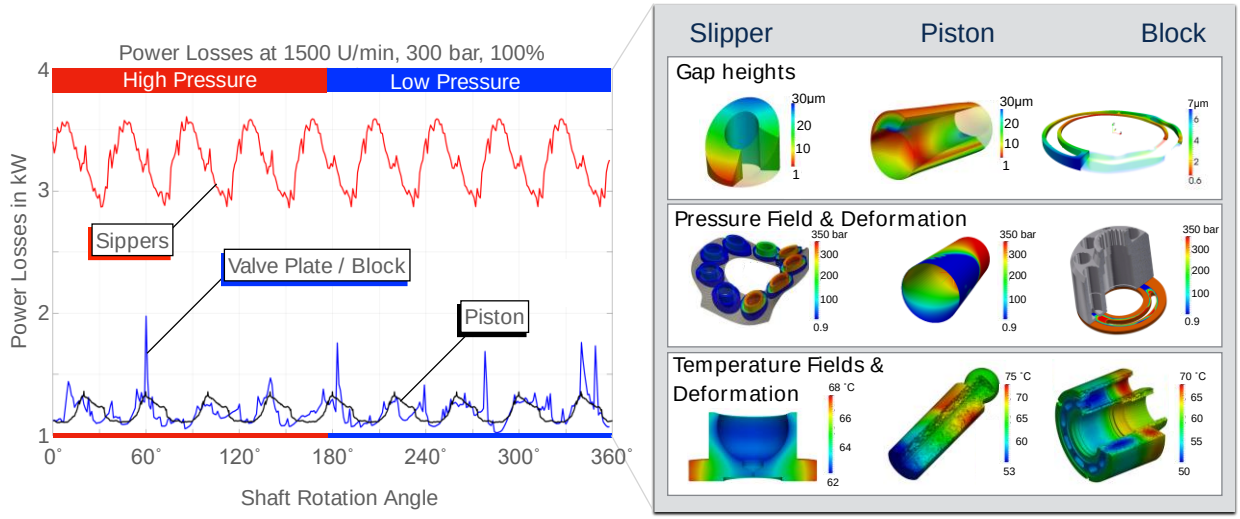

Figure 6: Outputs of the simulation including individual power losses.

For the forthcoming simulation results the following boundary conditions were used: The inlet temperature was kept constant at 35˚C, while the outlet and leakage temperature were set to the measured port temperatures. The integrated Caspar FSTI oil model for HLP46 was used, which is the oil in the utilized test rig. The resulting oil properties can be seen in **Figure 7** below. As depicted the model considers most oil property changes with respect to pressure and temperature. Only exception is the heat capacity of the oil which is kept constant at 2000 J/kg-K and the oil heat conductivity at 130 W/K.

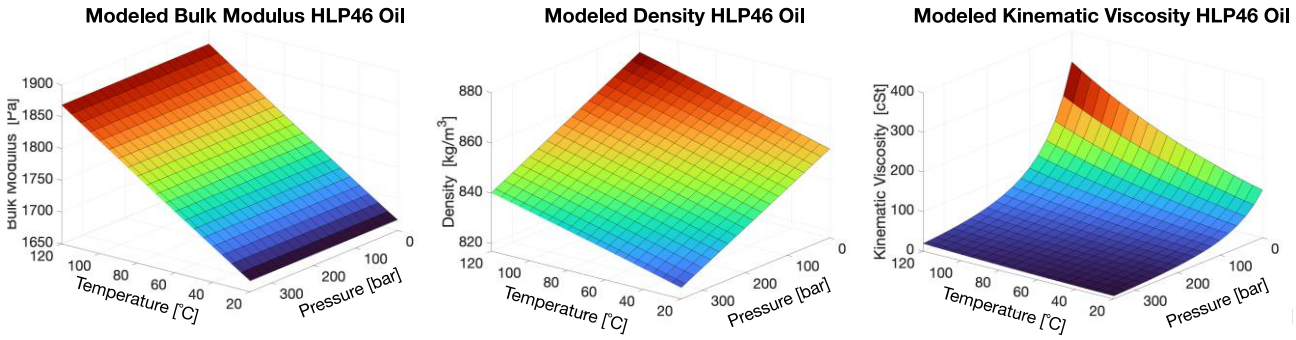

Figure 7: Modeled oil properties of typical HLP46 hydraulic oil.

4.2. Predicting wear to improve thermal forecast

In order to forecast the correct pump efficiency, it is crucial to include the worn-in pump parts, otherwise the simulation will overpredict the losses and temperature levels. Surface measurements are not always available; thus this section will illustrate how the simulation can predict the surface run-in and demonstrate the dramatic change in efficiency an temperature level, due to just a few micrometer of material abrasion. Figure 6 shows that the simulation predicts a much higher power loss at the slipper/swash plate interface for the given operating condition. The inputs were nominal part dimensions of the slipper along with a perfectly flat surface assumption. With these assumptions the simulation predicted contact during the high-pressure stroke not only for this pressure and speed level. **Figure 8** (left) shows the predicted slipper wear potential for various operating conditions. The speed increases from left to right, indicating that at low speed and high pressure as well as at high speed the slipper tends to wear in. In the plot on the top right, the average contact pressure in the fluid gap between slipper and swash plate is shown over one shaft rotation for 2100 rpm and 300 bar. The simulation predicts contact during the high-pressure stroke between 0-180˚. On the bottom right, contact pressure, fluid height and the pressure in the gap are shown for φ = 117˚, illustrating the contact location.

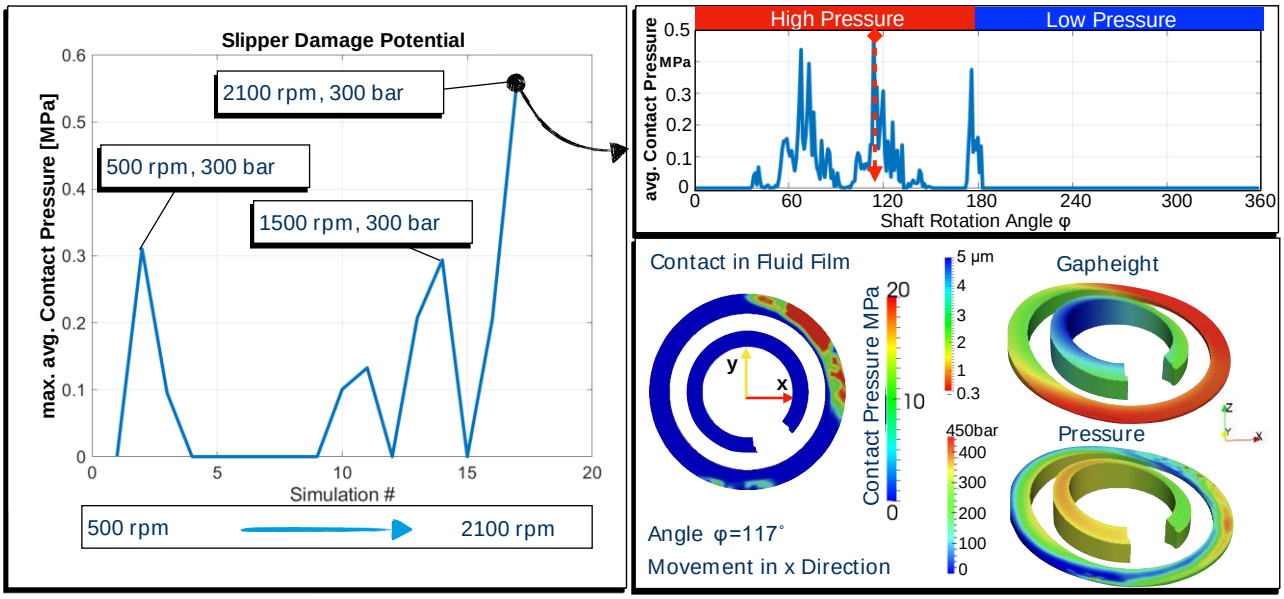

Figure 8: Slipper contact prediction.

The x-direction illustrates the movement direction, while the y-direction is the radial outwards direction, in which the centripetal force acts. As a result of this force slipper is tilted towards the inside edge, as indicated by the 3D gap height in the top right corner. Due to inadequate hydrodynamic pressure build-up, the gap height is very low during this point, causing a contact pressure on the leading edge of the slipper. This slipper has two sealing lands, the outer is the main seal, where the pressure drop from the pocket occurs, while the inner land is for hydrodynamic and structural purposes. Before the wear-in the slipper orientation is not beneficial for the inner edge, causing a low hydrodynamic built up. After the wear the slipper tilt changes, leaning more on the trailing edge.

This is illustrated by the 3D pressure field on the bottom of **Figure 9**. This figure shows the contact pressure for three wear stages on the top half: No wear, wear after 2 iterations, and contact prediction after the final wear profile is reached. The bottom right graph shows the material removal on the main sealing land as predicted by iterative simulation approach compared to a measured profile using a profilometer. The predicted wear matches reality quite well, indicating a 2 µm wear of at the outer edge of the sealing land. The used wear model, which uses the contact pressure and predicts the

material removal in µm, is described in detail in [3].

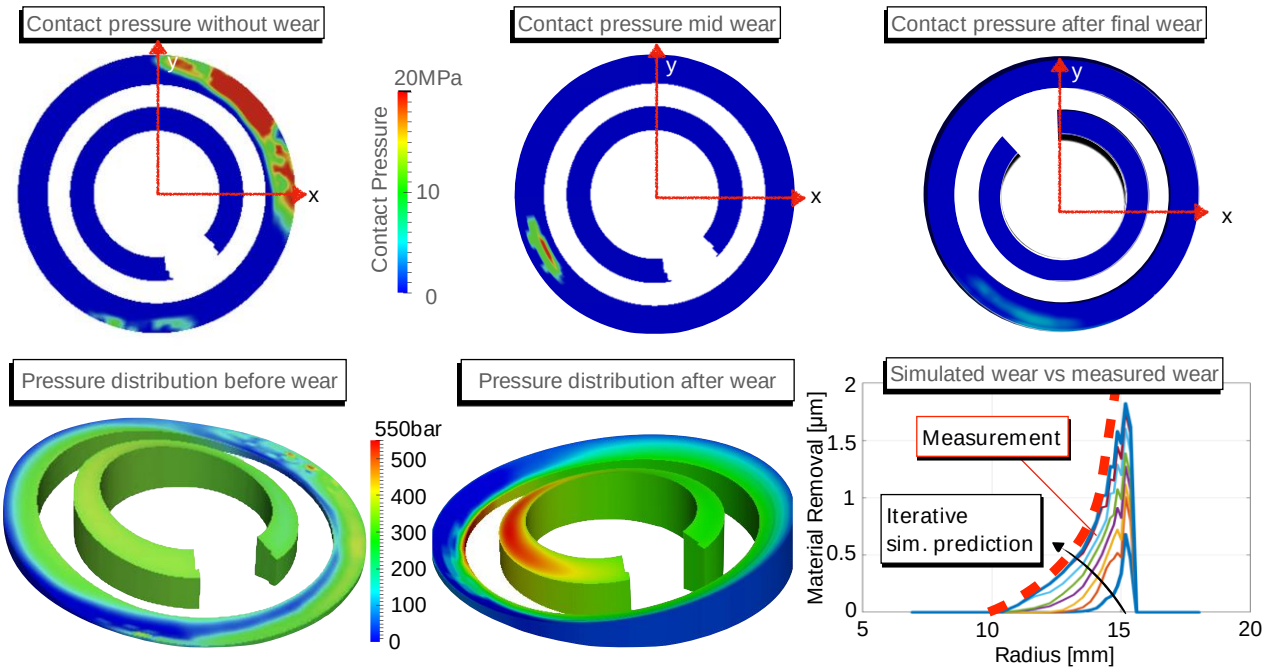

Figure 9: Wear prediction at the slipper using Caspar FSTI at 2100 rpm and 300 bar

On the bottom of Figure 9 is the 3D gap height with the pressure field for the non-worn slipper and the slipper with wear at 1500 rpm and 300 bar. The less then 2 µm rounding of the sealing land edge causes a shift in orientation, allowing the inner land of the slipper to build up a significant amount of pressure. This stabilizes the slipper, increases gap height to more efficient levels and prevents further wear. This change in orientation and gap height produces less viscous friction, reducing the powerlosses at 1500 rpm and 300 bar by 3 kW and the torque loss by more than 50%, as shown in **Figure 10**. The temperature level of the swash plate is greatly affected by the reduced power losses, dropping by more than 100 ˚C, which in turn reduces the leakage and retrospectively the entire cylinder block temperature. The temperature field of the swash plate is shown in **Figure 11**. This example demonstrates the importance to adequately model each gap, as they are all connected either directly or indirectly through the surrounding oil in the case.

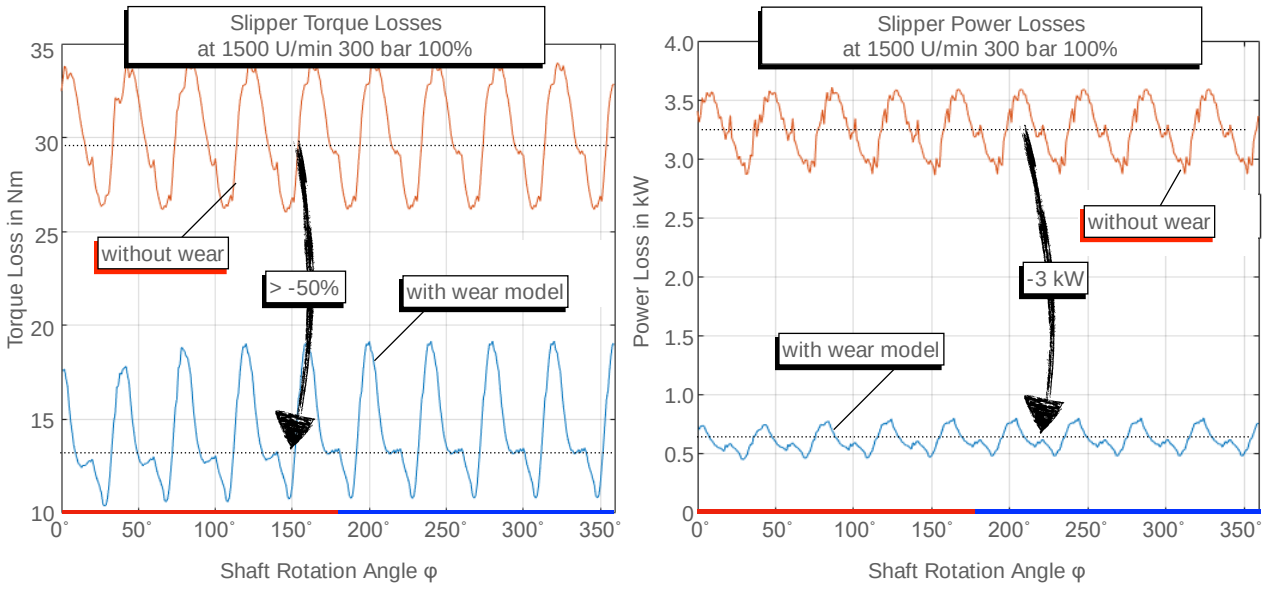

Figure 10: Simulated torque and power losses with and without wear modeled.

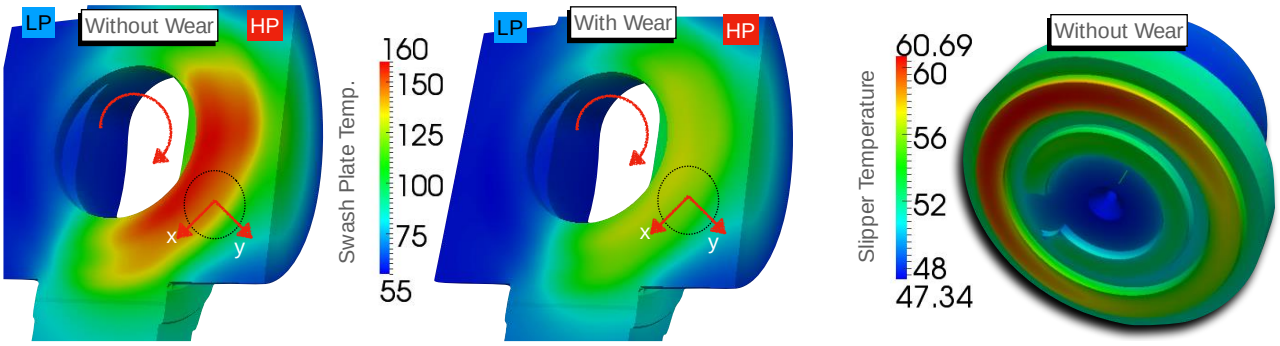

Figure 11: Predicted temperature with and without wear model at 1500 rpm and 300 bar.

Similar to the shown slipper case study, each surface pairing will be modeled, and wear was either predicted or measured and then accounted for. After all wear is accounted for, the entire operating range of the pump is simulated and analyzed. The results are presented in the following chapter, correlating the pump's efficiency with the cylinder block temperature.

4.3. Simulated correlation between efficiency and cylinder block temperature

Block temperature and pump efficiency are closely linked. For instance, elevated temperatures lead to reduced oil viscosities (refer to Figure 7), which could potentially increase leakage. Simultaneously, this reduced viscosity might decrease the oil's load-holding capacity, resulting in smaller gap heights. These lower gap heights, in turn, enhance viscous friction and diminish leakage, thereby raising the temperature. Furthermore, increased temperatures also cause thermal deformation of components, affecting the gap height as well. Despite these complexities, the trends shown subsequently are consistent and corroborated by the measurements detailed in chapter 5.2.

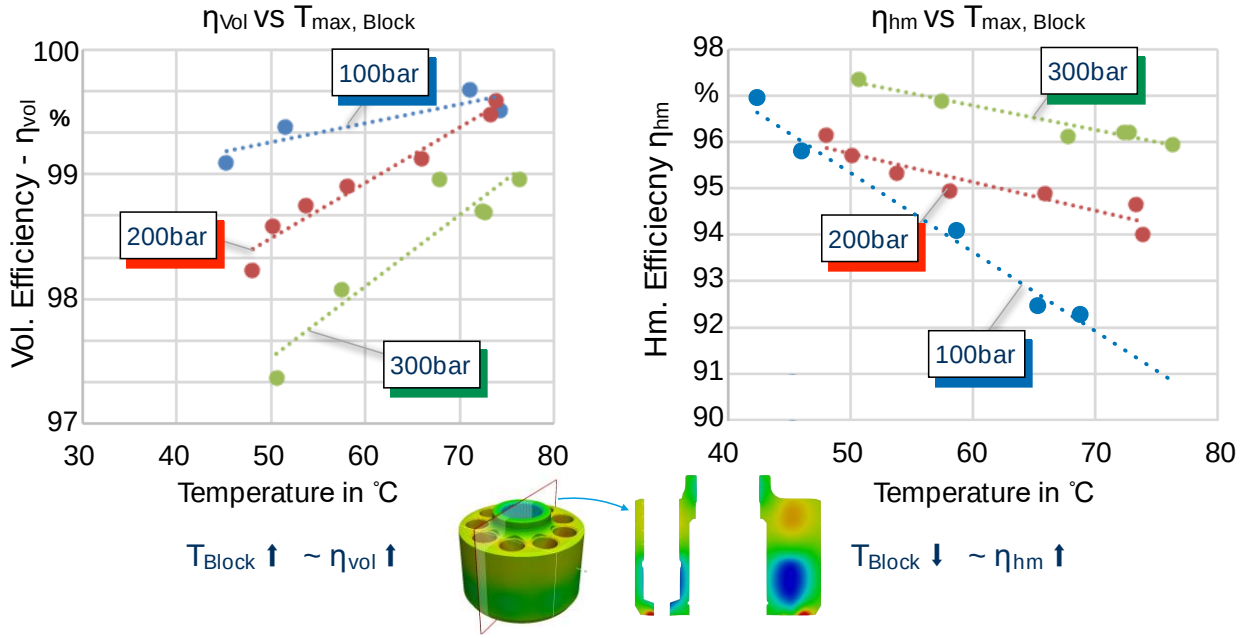

Figure 12: Simulated correlation between efficiency and cylinder block temperature

Figure 12 presents the simulation results for the maximum cylinder block temperature on the x-axis versus the volumetric (left) and hydromechanic efficiency (right) after accounting for all surface run-in. Each circle represents one operating condition, and they are color-coded to a pressure level. Blue dots show the temperature level and the partial pumps efficiency (η_{vol} or η_{hm}) for operating conditions at 100 bar, red 200 bar and green at 300 bar. The dotted lines show the linear fit for each pressure level, which demonstrates a distinct temperature corresponding to specific efficiencies. To facilitate

a clearer visualization, the data points have been plotted on a linear scale. However, it's noteworthy that the volumetric efficiency aligns more accurately with a logarithmic fit than a linear one. In terms of trends, the volumetric efficiency exhibits an upward trajectory, particularly at higher pressures. This pattern can be attributed to the cooling effect of the leakage flow. Essentially, greater leakage translates into more heat being carried away from the lubricating gaps, thus lowering the overall temperature of the part. Consequently, a higher volumetric efficiency, indicative of lower leakage, results in elevated temperatures.

Conversely, the trend observed with hydromechanical efficiency differs from that of volumetric efficiency. Higher hydromechanical efficiency is associated with reduced power losses due to friction, thus leading to lower temperatures.
The simulated pump efficiency compared to the measured efficiency of the pump can be seen in **Figure 13**. The simulated efficiency is based on the worn-in pump parts and the worn surface shapes. Left is the total efficiency at 100 bar and 250 bar plotted across the pumps speed range. The measured values are in the solid line and color coded to the pressure. Overall, the simulated efficiency matches the trend quite well, albeit it is higher than the measured. This is to be expected as not all loss sources are accounted for. When comparing the trend there is a close match between simulation and measurement for both pressure levels. The simulation correctly predicts the drop off at 250 rpm and 250 bar, as well as the trend with speed at the both pressure levels. This low-speed region showed the most significant changes when comparing simulation with and without wear. The differences in the efficiency magnitudes can be explained by the right side of the figure. Here the partial efficiencies at 100bar are shown for both measurement and simulation. As can be seen the volumetric efficiency is matched quite well. The discrepancy results in the hydrodynamic efficiency, which directly correlates to friction and torque losses. The simulation model predicts the losses in the lubricating gaps of the rotating group only, neglecting additional frictional losses in the roller bearings, the setting system and due to the oil churning in the housing. This claim can be supported by the fact, that the difference between the measured and simulated hydromechanical efficiency increases with speed, as the churning losses increase with the exponential of the speed, as shown in published models and measurements [35]–[37]. According to the CFD simulations (see Figure 21) the churning losses for this pump at 2100 rpm are close to 5.5 Nm. This amounts to about 2% additional losses in the hydromechanical efficiency at 100 bar, which is in agreement with the model of Bing [36]. Factoring in these churning losses in the hydromechanical efficiency result in the dotted line shown in the right figure.

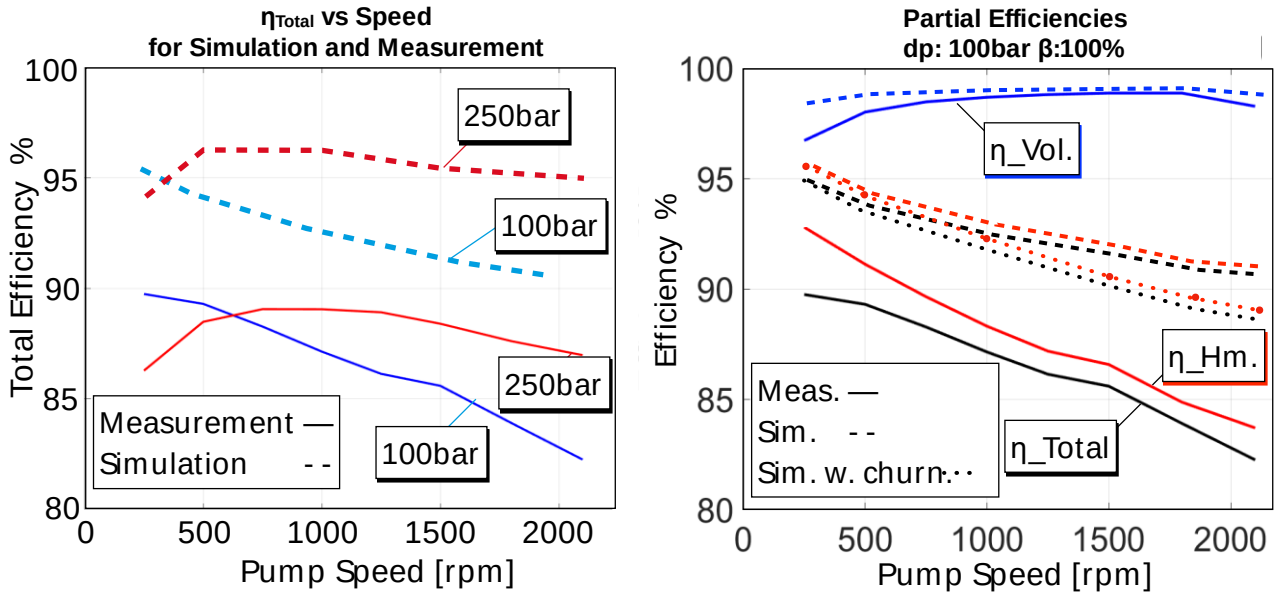

Figure 13: Simulations including wear vs measured efficiencies.

5. MEASUREMENT

To validate the predicted temperature-efficiency trends, it is necessary to measure the cylinder block temperature in a regular pump setting, without modifying crucial pump components, as has been done in the past [9], [29], [38]. To accomplish this, a special telemetric system was used, which can accurately measure a large number of sensors simultaneously. The system was originally developed to measure temperature and pressure in high speed turbine applications within an accuracy of ≦0.1K. The system was adapted to measure 24 thermocouples and 4 heat convection coefficient sensors, which are described in more detail in section 5.3.

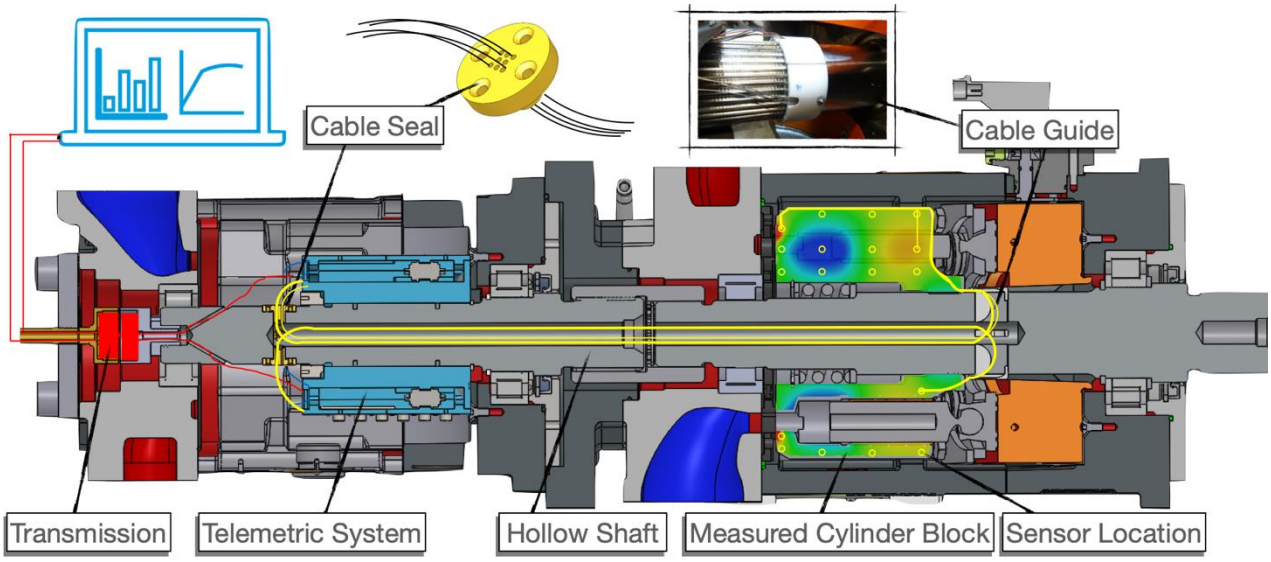

Figure 14: Measurement Set Up

The set up can be seen in **Figure 14**, where a tandem pump arrangement was used to mount and house the telemetric system to the 160cc open circuit pump, while the test pump is shown on the right, with the tested cylinder block highlighted. The sensor locations and temperature field are illustrated, with the exact sensor locations shown in Figure 16. The sensor cables are guided from the cylinder block through hollow shafts using 3D printed parts to guide the cables during pump assembly. In order to seal the case properly the cables were individually guided through a cable seal, that was then sintered shut. The used thermocouples were of type K with metal mantle, which allowed them to be sintered into the cylinder block. The telemetric system converts the analog temperature signals to digital bits that can be transmitted wirelessly to the acquisition system. The power is also transmitted through this brushless system. This set up allows for a very reliable and accurate measurement, not only of temperature but also other signals. In future publications simultaneous pressure and temperature measurements will be shown, that were recorded using this set up.

Next to the cylinder block's temperature, the pump is also monitored holistically with an array of sensors, as shown in **Figure 15**. Each fluid line is equipped both with pressure and temperature sensors, where the temperature is recorded with industrial as well as high accuracy thermistors. The housing of the pump is equipped with 5 temperature sensors and a thermal camera recorded the temperature distribution. As the run-in process and the local temperature are in correlation, the pump was also monitored for particles emitted. The suction line was also equipped with a transparent section that allows for visual inspection of air bubbles, to ensure for a cavitation free operation.

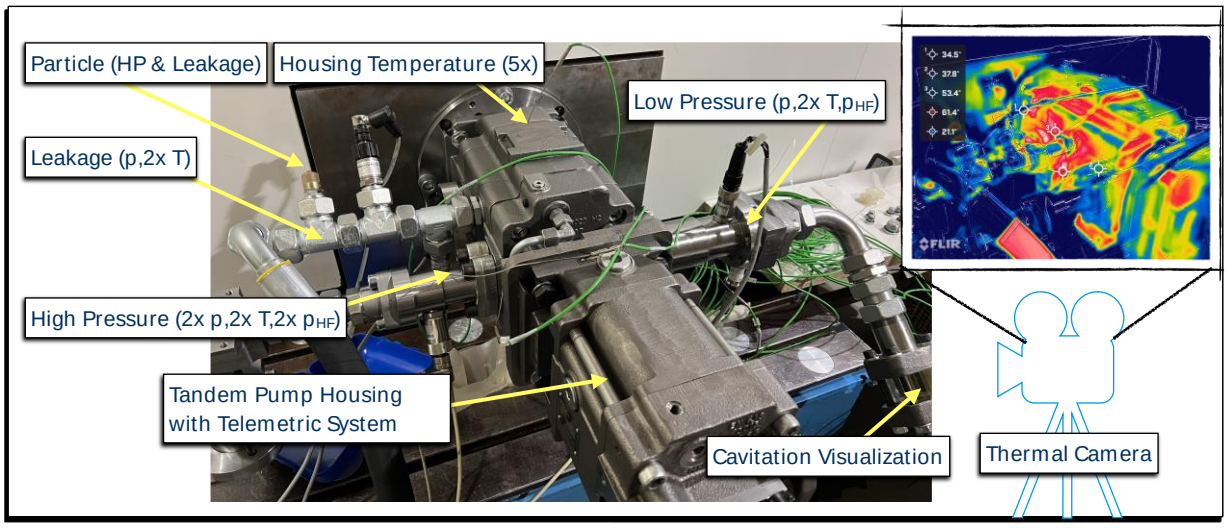

Figure 15: External sensors on the test pump.

5.1. Cylinder block temperature measurements

Figure 16 showcases a sample result for a high-speed operating condition. Here, the simulated outcomes (on the left) can be compared to the measurements (on the right and in the table). For the specific operating parameters of 2100 rpm, 200 bar, and 100% displacement, the pump remained inactive for over 24 hours, essentially reverting to room temperature before initiating the test. Following this, there was a gradual ramp-up, with speed escalating from 0 to 2100 rpm within approximately 10 seconds and pressure surging from 0 to 200 bar within a similar timeframe.

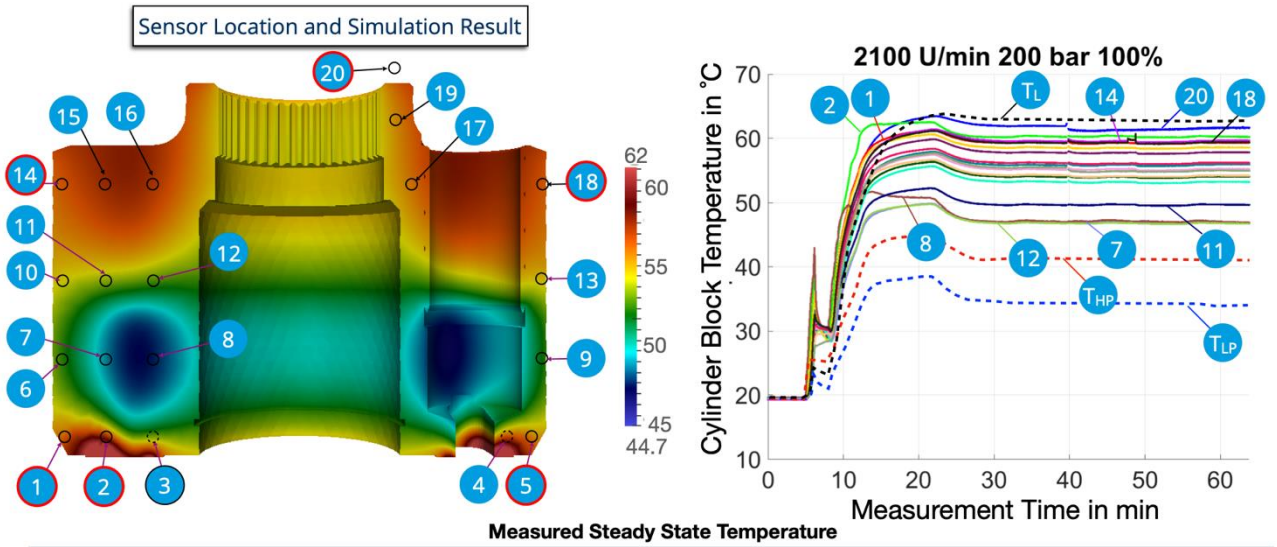

Measured Steady State Temperature

T_{LP}	T_{HP}	T_L	S1	S2	S5	S6	S7	S8	S9	S10	S11	S12	S13	S14	S15	S16	S17	S18	S19	S20
35.0	42.1	62.8	60.4	61.3	59.6	55.1	47.9	48.0	54.3	57.0	50.7	47.8	56.3	60.7	58.9	57.3	55.3	60.5	56.1	62.7

Figure 16: Measured and simulated cylinder block temperatures at 2100 rpm, 200 bar and 100% disp.

One notable observation is the swift temperature response in the cylinder block, registering changes in 15 s. However, attaining thermal equilibrium across the entire pump—where all components stabilize, and the desired inlet temperature is met (with a margin of ±1K)—takes close to an hour. It should be noted that this time frame corresponds to a cold start, condition changes when the pump reached operating temperatures usually reach thermal equilibrium within 10-20 min. All measurements were aimed to be taken at 35˚C inlet. Small deviations were later corrected to make

the results comparable between operating conditions.

Looking at the measured temperature distribution (right) and the simulated (left) in Figure 16, a good match between simulation and measurement can be seen. The predicted 15K temperature difference in simulation matches almost the 13.5 K measurement. The sensors were placed 5 mm away from the bottom cylinder block surface, as FEM fatigue calculations predicted a negative trend drilling the holes any closer. This could explain the difference in the maximal temperatures. The highest temperature is registered at sensor 2. These high temperatures at the bottom of the block predict higher viscous losses at the valve plate interface and the other high temperatures are at the top of the cylinder block (sensor 14 & 18), close to the top of the piston / bushing pairing. The piston has a high inclination at these speeds and pressures with its lowest gap height at the top of the bushing, explaining the hot spot. The low spots are at sensor 7 and 8, which are the closest to displacement chamber, which acts in a cooling manner. Sensor 20 was placed outside of the block directly in the leakage oil around the block. It is even hotter than the block, predicting that the hottest region is in fact in the gap and that the block is heated also from the surrounding oil and not just from the gaps.

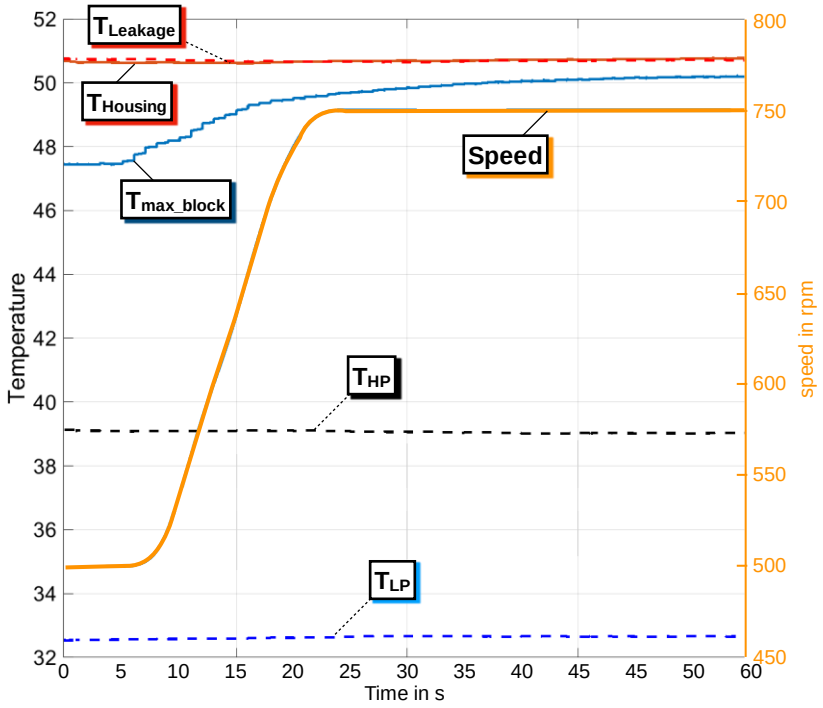

Figure 17: Temperature response rate of the cylinder block

To demonstrate that the cylinder block is better suited for the thermal monitoring as compared to the fluid temperature or the housing, **Figure 17** should be inspected. It shows a speed change from 500 to 750 rpm during warm conditions and the corresponding fluid temperature in the ports, housing temperature and the block temperature. The maximal block temperature (T_{max}) has an instant reaction to the speed change, rising 3˚C in 10s. Contrarily, other fluid and body temperature readings, such as those of the inlet, outlet, housing, and leakage, remain largely consistent in the given time frame despite the speed variation. This emphasizes the significance of the cylinder block temperature and underscores the advantage of in-pump measurements.

Preliminary studies suggest that this immediate temperature spike can potentially be harnessed to predict steady-state temperatures, paving the way for a more industrially relevant monitoring approach. Nevertheless, given that the simulation resides in a steady state, achieving this state in real-time measurements is paramount for meaningful comparisons.

5.2. Predicting the pumps efficiency with temperature measurement

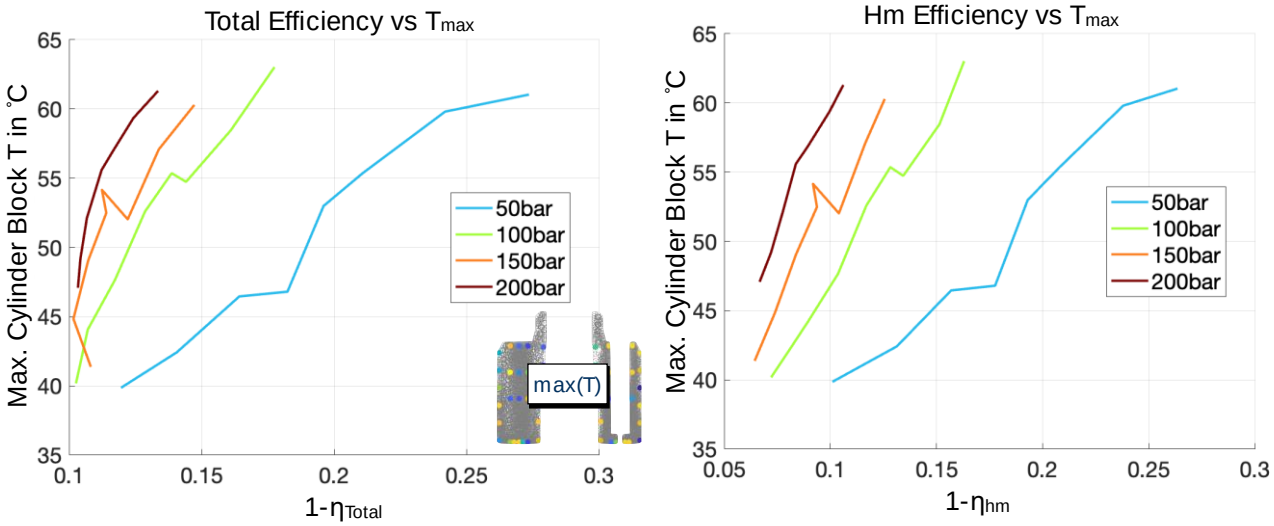

Figure 18: Measured trend between maximum block temperature and total (left) and hydromechanical (right) efficiency at 35˚C inlet.

Figure 18 shows the measured relationship between efficiency and block temperature at 35˚C inlet temperature (as is true for all following graphs). Left in the figure is the maximum cylinder block steady state temperature T_{max} and the total efficiency loss ($1-\eta_{total}$) for each pressure region. Although the pattern isn't strictly linear, distinct zones emerge for each pressure level. At 50 bar, the temperature increase appears to have a linear correlation with efficiency loss, suggesting that it's primarily driven by viscous losses. However, as pressures elevate, volumetric losses start to play a more prominent role. The linear relationship between viscous losses and the temperature can be confirmed by the right graph in the figure, which shows T_{max} vs $1-\eta_{hm}$. There is a clear linear trend for each pressure level. Linear trends are easily modeled and can be very helpful in prediction. Quadratic relationships can be helpful if the entire modeling region is known. The volumetric efficiency and the temperature seem to have such a quadratic relationship, as can be confirmed by the minimal surface temperature and the volumetric efficiency in **Figure 19**.

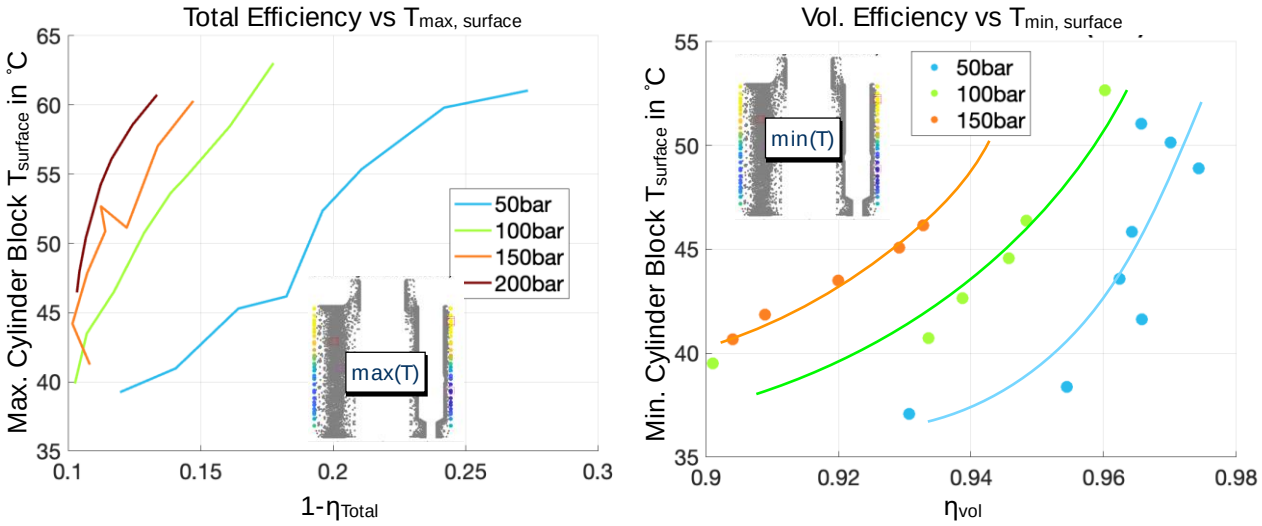

Figure 19: Total (left) and volumetric (right) efficiency trends with max and min block *surface* temperature.

This quadratic relationship of temperature and volumetric efficiency is shown on the right side of the figure for three pressure levels. This trend can be explained by the relationship between leakage flow increases and the gap height, as the flow increases with the height squared. Moreover, the figure

underscores that merely gauging the surface temperature suffices to forecast the pump's total efficiency. This is exemplified in the left graph, where the peak surface temperature is plotted against 1-ηtotal, revealing a similar pattern to what's observed in Figure 18. While the measured efficiencies and temperatures are different in magnitude at the current simulation stage, they still match in trend, confirming the simulated predictions. It is worth mentioning that while the maximum surface temperature can also be correlated with the volumetric efficiency, it was better and clearer trend utilizing the minimum temperature. When correlating the T_{max} with the volumetric efficiency the trend is comparable to the one shown in Figure 20.

Another interesting beneficial correlating the pumps efficiency with the block surface temperature, is the prediction of the pump's speed limit for each pressure level. In **Figure 20** the plot of mean surface temperature against the loss in volumetric efficiency ($1-\eta_{vol}$) reveals a noticeable deviation from the quadratic trend at specific temperatures for all pressure levels. Typically, temperature rises with an increase in volumetric efficiency. Yet, beyond a particular temperature threshold, despite a continuing rise in temperature, the volumetric efficiency starts to decline. Detailed analysis highlighted that this phenomenon emerges when the pump operates at exceedingly high speeds, nearing its maximum permissible speed.

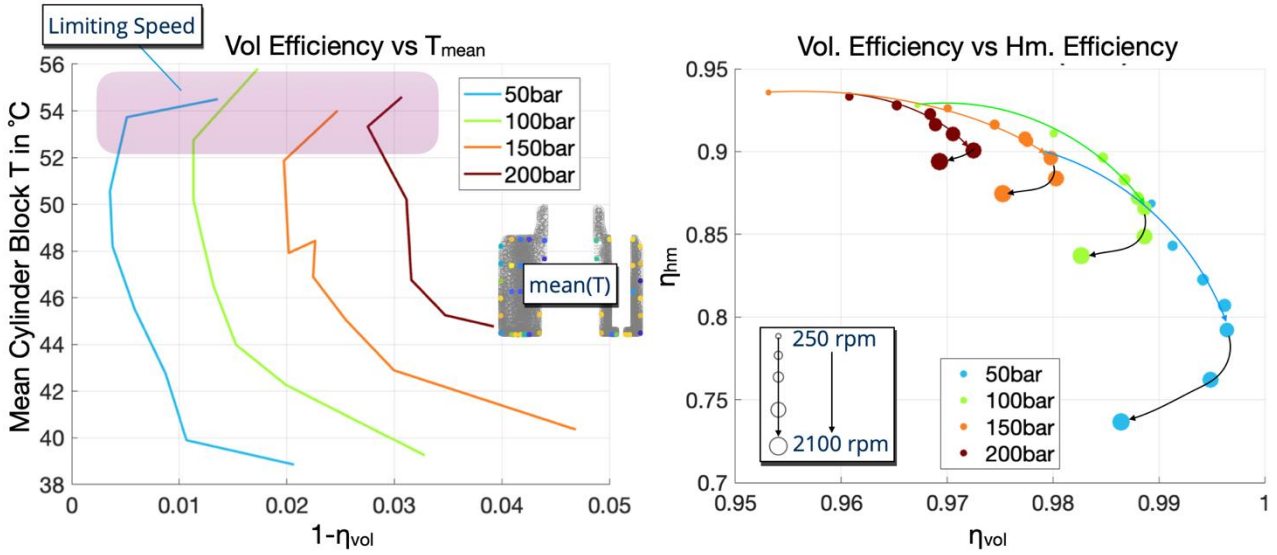

Figure 20: Limiting pump speed as per temperature and efficiency.

This observation is more pronounced when comparing volumetric efficiency to hydromechanical efficiency, as depicted on the right side of Figure 20. The plot shows each measurement point color coded with pressure and the size of the dot related the pump speed from 250-2100 rpm. During normal operation the volumetric efficiency η_{vol} increases with speed while the hydromechanical efficiency η_{hm} decreases. As can be seen this happens in a quite predictable fashion. The trend breaks at high speed when the η_{vol} drops while the η_{hm} drops as well. Notably, the speed at which this occurs varies with the pressure level: it's more immediate at lower pressures compared to higher ones. It will be further investigated if this trend can be detected with the temperature only, but initial trends suggest that it is detectible by comparing inlet, outlet and block temperature rise. This will give the installation of a block temperature a further incentive, being able to predict speed limits in open circuit pumps can be a crucial feature.

5.3. Measuring the heat convection coefficient

In Caspar's thermal modeling, key boundary conditions encompass the oil temperature, operational parameters, and the heat convection coefficient between the component's surface and the oil. While the oil temperature in the outlet and leakage channels can be directly gauged, it can also be estimated

based on pressure and anticipated efficiency, as noted in [39]. Caspar's simulation can ascertain efficiency using an initial approximation, which is then iteratively refined with each subsequent simulation. However, the heat convection coefficient remains a largely unexplored variable in hydraulic pump modeling due to a lack of prior measurements. Historically, computational fluid dynamics (CFD) tools were utilized to estimate this coefficient. Yet, such predictions were grounded in numerous assumptions, and in the absence of direct measurement, a validation was not available.

Uffrecht et. al. [16], [17], [40] were able to develop a miniature sensor, which was able to measure this coefficient. The sensor consists of a thermistor that can simultaneously be used as a heating element, all while being insulated from the surrounding material. The equation of for the heat transfer is given in Eq. 1 below. With a known current the heat loss Q is known, using an insulated material the area A is known as well. To determine the heat convection coefficient h is necessary to measure the temperature ΔT, which is the body surface temperature T and the surrounding Temperature T_{inf}. The sensor accomplishes this by acting as both the heat source and the temperature sensor itself. When powered only a short time the temperature can be measured, and by continuously powering the sensor it will heat up.

$$Q = h \cdot A \cdot \left(T - T_{inf}\right) \tag{1}$$

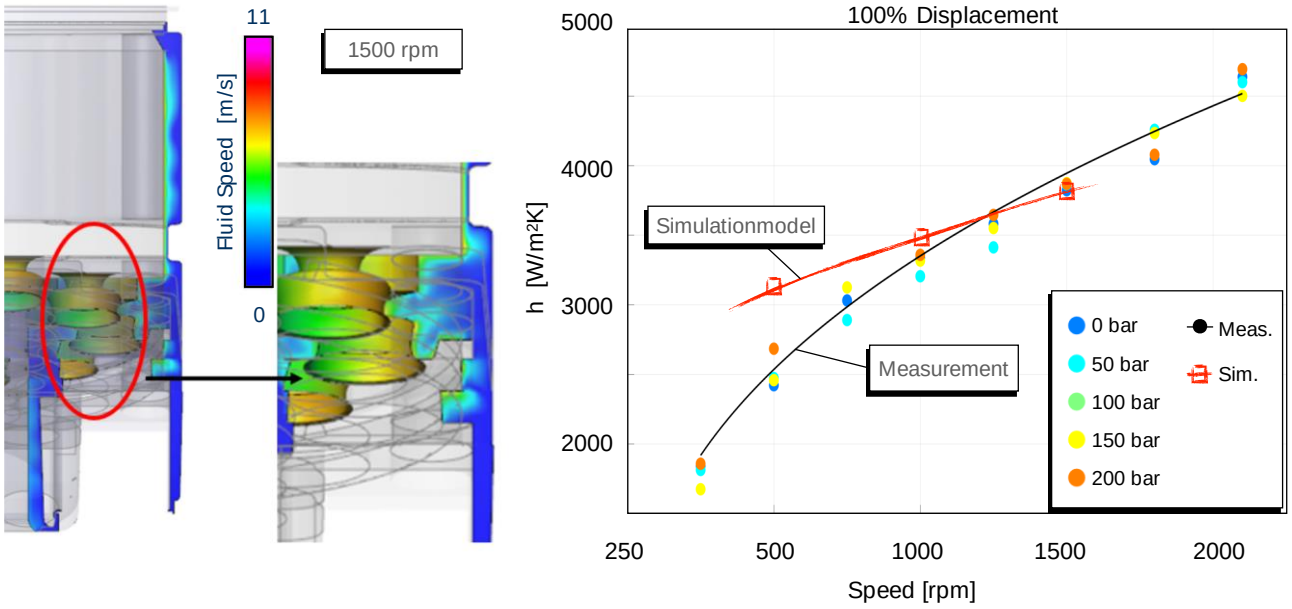

Figure 21: Measured heat convection coefficient of the cylinder block outer surface at 100% displacement vs simulation.

Four of such sensors were placed on the cylinder block wall, two at the outer diameter and two at the neck. The idea was to confirm the different heat convection coefficients at different radii and therefore at different fluid speeds. The neck region is also surrounded by moving pistons, which cause a significant turbulence as predicted by the CFD model shown in **Figure 21** on the left. The CFD simulations were made with Simerics MP+. The model prediction at 100% displacement at three different speeds are shown on the right in red. The measurements at 5 different pressure levels are also shown. It can be seen, that the CFD simulation and the measurement do match in certain regions, however there is a slight difference in slope due to a worse match at low speeds. Nevertheless, these measurements confirm that CFD tools are capable of predicting the heat convection coefficient, as small deviations in the h-coefficient don't have a significant impact on the result. Some CFD models however precited values a full magnitude above these levels, hence it was necessary to validate these numbers.

Figure 21 reveals that pressure variations minimally impact heat convection, with measurements clustering closely for each speed. It also verifies that the sensor delivers reliable results and works well at different thermal loadings of the block.

Figure 22 illustrates how the swash plate angle and block surface influence the convection coefficient. Here the results from 3 of 4 installed sensors are shown, unfortunately did one of the sensors placed on the outer block wall stopped working shortly after commissioning the pump. The 3 remaining sensors are shown in different colors. In green and red are the sensors placed at the neck and in blue the sensor on the outer surface. A dotted line represents 50% swash plate angle, while 100% represents full displacement. The displacement seems indifferent to the heat convection of the outer surface, as evidenced by the overlapping data lines, attesting to the measurement's precision. Both Neck1 (red) and Neck 2 (green) display a noticeable effect from the swash plate angle, with 'h' rising correspondingly. This can be explained by the fact that a lower angle increases the total surface area of the piston exposed to the surrounding oil, increasing drag and turbulence and therefore the heat convection. This effect was first shown in [36], [41] for the churning losses.

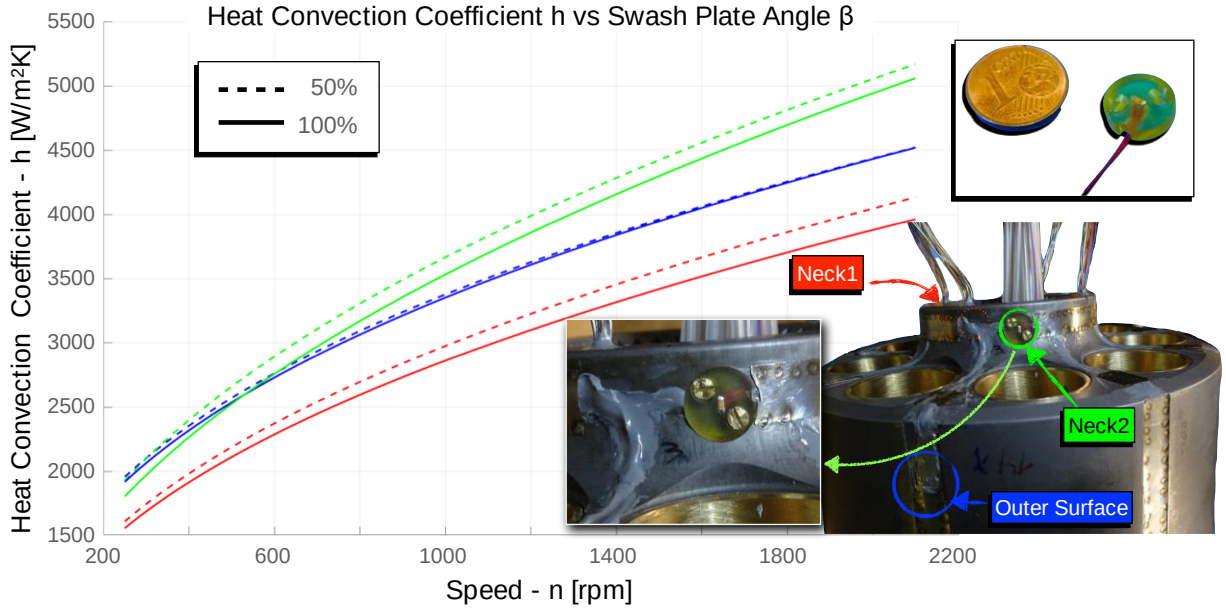

Figure 22: Measured h of the cylinder block at different locations and displacements.

The results of the Neck1 sensor with respect to the outer surface sensors show the expected results. As the rotational radius decreases the fluid speed also decreases, which leads to smaller heat convection coefficients, however the overall trend remains the same just with an offset. The Neck2 sensor diverges in its trend and notably exceeds the magnitudes of the other two sensors. The cause for this deviation is due to a small collection of glue right before the sensor, which was used to guide and protect the cables, see bottom of Figure 22. This caused the oil flow to become turbulent and therefore increase h. Plans are underway to replicate these tests using four new sensors and special care will be taken to avoid surface topological changes with the cable guidance, aiming to validate this hypothesis.

6. CONCLUSION AND OUTLOOK

The intricate relationship between the steady state temperature of a cylinder block in an axial piston pump and its total, volumetric and hydromechanical efficiency forms the core of this investigation, revealing insights that echo and solidify findings previously derived from simulation analyses. Harnessing the capability of the Caspar FSTI—a validate simulation software renowned for its ability

to predict losses in axial piston pumps—the paper revealed a correlation consistent with those previously detected for a 92cc pump from an alternative manufacturer – then in simulation only [1]. This resonant correlation stands testament to the versatility and universality of the observed temperature-efficiency relationship across different pump capacities and potentially, manufacturing intricacies.

A prominent feature of this study was the strategic placement of 24 temperature sensors across 20 distinct positions within a cylinder block, guided strictly by insights drawn from the simulation model. This approach was instrumental in capturing nuanced temperature profiles, thus allowing for an enriched understanding of the internal thermal dynamics. Further enhancing the credibility and accuracy of the empirical process was the incorporation of a specialized telemetric system. This system, known for its precision, enabled real-time transmission of data from both the temperature sensors and the four additional sensors dedicated to measuring heat convection coefficients.

The measurement matches the simulation quite well at many operating conditions, predicting both hot and cold spots, as well as the temperature range within a reasonable accuracy. The empirical findings, when compared with the simulated trends, not only validate the latter's credibility but also shed light on previously uncharted terrains of axial piston pump temperature behavior. For instance, a noteworthy revelation pertains to the pump's behavior upon approaching its limiting speed, providing a fresh perspective into the operational constraints, and associated thermal implications.

In the next steps of this research endeavor the measurements will be repeated with all new parts, which were not previously run-in at the manufacturers end-of line test. This should give additional insight into the thermal effects during the pumps first hours and effect of wear on efficiency and temperature. Furthermore, the cylinder block will be equipped with even more sensors such as pressure and temperature inside the piston chamber.

The ability to predict efficiency using steady-state surface temperatures, combined with the block temperature's rapid response to the pump's operational changes, lends credence to the notion that this method is viable for real-time condition monitoring in axial piston pumps. Moreover, this can be achieved without compromising the block's durability or the overall integrity of the pump. In line with this, a wireless sensor is currently under evaluation and will be tested soon. This sensor can be effortlessly mounted on the surface without necessitating any wired connections. Both power and data transfers are executed wirelessly through a straightforward receiver located inside the pump housing.

Lastly, a focal area for further exploration is the relationship between temperature and efficiency trends. Current findings rely on steady state measurements which are time-consuming. However, preliminary investigations suggest that the steady state temperature may be estimated using an exponential function based on a mere 15 seconds of data. If validated, this approach could significantly enhance the applicability of the research results in real-world scenarios.

NOMENCLATURE

A	Area	m^2
β	Swash plate angle	°
ΔT	Differential temperature	K
φ	Shaft angle	°
h	Heat convection coefficient	W/m^2K
HP	High pressure	
n	Speed of the pump	rpm
η_{vol}	Volumetric pump efficiency	
η_{hm}	Hydromechanical pump efficiency	
η_{total}	Total pump efficiency	
LP	Low pressure	
T	Temperature	˚C
T_{in}	Inlet temperature	˚C
T_{max}	Maximum temperature of the cylinder block	˚C
T_{min}	Minimum temperature of the cylinder block	˚C
T_{mean}	Mean temperature of the cylinder block	
p	Pressure	bar
p_{HF}	High frequency pressure transducer	
P_{out}	Output power	kW
Q	Heat Flow	W

REFERENCES

[1] A. Shorbagy, R. Ivantysyn, F. Berthold, und J. Weber, „Holistic analysis of the tribological interfaces of an axial piston pump - Focusing on pump ' s efficiency“, in *IFK2022*, Aachen, 2022.

[2] R. Ivantysyn, A. Shorbagy, und J. Weber, „An approach to visualize lifetime limiting factors in the cylinder block/valve plate gap in axial piston pumps“, in *ASME/BATH 2017 Symposium on Fluid Power and Motion Control, FPMC 2017*, 2017. doi: 10.1115/FPMC2017-4327.

[3] R. Ivantysyn, A. Shorbagy, und J. Weber, „Investigation of the Wear Behavior of the Slipper in an Axial Piston Pump by Means of Simulation and Measurement“, in *12. IFK 2020*, 2020.

[4] R. Ivantysyn und J. Weber, „Investigation of the Thermal Behavior in the Lubricating Gap of an Axial Piston Pump with Respect to Lifetime“, in *11. IFK 2018*, 2018.

[5] R. Ivantysyn und J. Weber, „“Transparent Pump” – An approach to visualize lifetime limiting factors in axial piston pumps“, in *ASME 2016 9th FPNI Ph.D Symposium on Fluid Power*, Florianapolis, Brazil, 2016.

[6] R. Ivantysyn, A. Shorbagy, und S. Schmatz, „Smart Pump – Decentralised control for vessel engine“, 2018.

[7] S. Horn, R. Ivantysyn, und J. Weber, „Validated efficiency improvements by implementation of structures on the slipper surface of an axial piston pump“, in *IEEE GFPS 2022*, Naples, 2022.

[8] U. Wieczorek, „Simulation Of The Gap Flow In The Sealing And Bearing Gaps Of Axial Piston Machines“, *Proceedings of the 1st FPNI PhD Symposium*, S. 493–507, 2000.

[9] M. Pelosi, „An Investigation on the Fluid-Structure Interaction of Piston/Cylinder Interface“, Purdue University, 2012.

[10] A. Schenk, „Predicting Lubrication Performance Between the Slipper and Swashplate in Axial Piston Hydraulic Machines“, Purdue University, 2014.
[11] M. Zecchi, „A novel fluid structure interaction and thermal model to predict the cylinder block/valve plate interface performance in swash plate type axial piston machines“, Purdue University, West Lafayette, IN, 2013. Zugegriffen: 20. August 2014. [Online]. Verfügbar unter: http://gradworks.umi.com/36/13/3613547.html
[12] G. Schroeder und W. Uffrecht, „A new test rig for time-resolved pressure measurments in rotating cavities with pulsed inflow“, in *ASME Turbo Expo 2010*, 2010, S. 1–10.
[13] W. Uffrecht und E. Kaiser, „Influence of force field direction on pressure sensors calibrated at up to 12,000 g“, *J Eng Gas Turbine Power*, Bd. 130, Nr. 6, S. 1–8, 2008, doi: 10.1115/1.2966390.
[14] B. Heinschke, W. Uffrecht, A. Günther, S. Odenbach, und V. Caspary, „Telemetric measurement of heat transfer coefficients in gaseous flow - First test of a recent sensor concept in a rotating application“, *Proceedings of the ASME Turbo Expo*, Bd. 6, S. 1–10, 2014, doi: 10.1115/GT2014-26239.
[15] W. Uffrecht und A. Günther, „Electro-thermal measurment of heat transfer coefficients“, in *ASME Turbo Expo 2012*, 2012.
[16] W. Uffrecht, A. Günther, und V. Caspary, „Kleine Thermistoren zur messung von wärmeübergangskoeffizienten“, *Technisches Messen*, Bd. 79, Nr. 12, S. 549–558, 2012, doi: 10.1524/teme.2012.0230.
[17] G. Eschmann, A. Kuntze, W. Uffrecht, und S. Odenbach, „Measurement if heat transfer coefficients un gaseous flow - first test of a recent sensor concept for stationary and oscillating flow“, in *ASME Turbo Expo 2014*, 2014, S. 1–11.
[18] W. M. J. Schlösser und K. Witt, „Thermodynamisches Messen in der Ölhydraulik“. VDMA, 1976.
[19] K. Witt, „Thermodynamisches Messen in der Ölhydraulik : Einführung und Übersicht. “, *Oelhydraulik und Pneumatik*, Bd. 20, Nr. 6, S. 416–424, 1976.
[20] H. J. Matthies und K. T. Renius, *Einführung in die Ölhydraulik*. 2014. doi: 10.1007/978-3-658-06715-1.
[21] K. T. Renius, „Experimentelle Untersuchung an Gleitschuhen von Axialkolbenmaschinen“, *O + P : Zeitschrift für Fluidtechnik*, Bd. 17, Nr. 3, S. 75–80, 1973.
[22] K. T. Renius, „Untersuchungen zur Reibung zwischen Kolben und Zylinder bei Schrägscheiben-Axialkolbenmaschinen“, *VDI Forschungsheft*, 1974.
[23] D. S. Wegner und F. Löschner, „Validation of the physical effect implementation in a simulation model for the cylinder block / valve plate contact supported by experimental investigations“, in *IFK2016*, 2016, S. 275–287.
[24] J. Kim und J. Jae-Youn, „Measurement of Fluid Film Thickness on the Valve Plate in Oil Hydraulic Axial Piston Pumps (Part I)“, *KSME International Journal*, Bd. 17, Nr. 2, S. 246–253, 2003, [Online]. Verfügbar unter: http://www.dbpia.co.kr/Journal/ArticleDetail/3227503
[25] J. M. Bergada, J. Watton, und S. Kumar, „Pressure, Flow, Force, and Torque Between the Barrel and Port Plate in an Axial Piston Pump“, *J Dyn Syst Meas Control*, Bd. 130, Nr. 1, S. 011011, 2008, doi: 10.1115/1.2807183.
[26] C. J. Hooke, „The lubrication of overclamped slippers in axial piston pumps—centrally loaded behaviour“, *Proc Inst Mech Eng C J Mech Eng Sci*, Bd. 202, Nr. 4, S. 287–293, 1988, doi: 10.1243/PIME_PROC_1988_202_121_02.

[27] C. J. Hooke, „The effects of non-flatness on the performance of slippers in axial piston pumps“, *Proc Inst Mech Eng C J Mech Eng Sci*, Bd. 197, Nr. 4, S. 239–247, 1983, doi: 10.1243/PIME_PROC_1983_197_104_02.
[28] N. D. Manring, C. L. Wray, und Z. Dong, „Experimental studies on the performance of slipper bearings within axial-piston pumps“, *J Tribol*, Bd. 126, Nr. 3, S. 511–518, 2004, doi: 10.1115/1.1698936.
[29] T. KAZAMA, T. TSURUNO, und H. SASAKI, „Temperature Measurement of Tribological Parts in Swash-Plate Type Axial Piston Pumps“, *Proceedings of the JFPS International Symposium on Fluid Power*, Bd. 2008, Nr. 7–2, S. 341–346, 2008, doi: 10.5739/isfp.2008.341.
[30] P. Achten und S. Eggenkamp, „Barrel tipping in axial piston pumps and motors“, *Proceedings of 15:th Scandinavian International Conference on Fluid Power, 15th Scandinavian International Conference on Fluid Power, Fluid Power in the Digital Age, SICFP'17, June 7-9 2017 - Linköping, Sweden*, Bd. 144, S. 381–391, 2017, doi: 10.3384/ecp17144381.
[31] S. Wegner, „Experimental investigation of the cylinder block movement in an axial piston machine“, in *FPMC2015 -9529*, 2015.
[32] H. Xu *u. a.*, „The direct measurement of the cylinder block dynamic characteristics based on a non-contact method in an axial piston pump“, *Measurement (Lond)*, Bd. 167, Nr. April 2020, 2021, doi: 10.1016/j.measurement.2020.108279.
[33] A. Shorbagy, R. Ivantysyn, und J. Weber, „An experimental approach to simultaneously measure the temperature field and fluid film thickness in the cylinder block/valve plate gap of an axial piston pump“, in *Turbulence, Heat and Mass Transfer 9*, 2018.
[34] U. Wieczorek und M. Ivantysynova, „Computer aided optimization of bearing and sealing gaps in hydrostatic machines—the simulation tool caspar“, *International Journal of Fluid Power*, Bd. 3, Nr. 1, S. 7–20, 2002, doi: 10.1080/14399776.2002.10781124.
[35] Y. Li, B. Xu, J. H. Zhang, und X. Chen, „Experimental study on churning losses reduction for axial piston pumps“, *11th International Fluid Power Conference*, S. Vol. 272-280, 2018.
[36] X. Bing, „Modeling and Analysis of the Churning Losses Characteristics of Swash Plate Axial Piston Pump“, *2015 International Conference on Fluid Power and Mechatronics (FPM)*, S. 22–26, 2015, doi: 10.1109/FPM.2015.7337078.
[37] W. Chunhui, „Analysis of churning Losses of Axial Piston Pump Rotating Parts Based on the Moving Particle Semi Implicit Method“, *Int J Heat Mass Transf*, 2021.
[38] L. Olems, „Investigations of the Temperature Behaviour of the Piston Cylinder Assembly in Axial Piston Pumps“, *International Journal of Fluid Power*, Bd. 1, Nr. 1, S. 27–38, 2000, Zugegriffen: 19. August 2014. [Online]. Verfügbar unter: http://www.tandfonline.com/doi/abs/10.1080/14399776.2000.10781080
[39] J. Schlösser, „Thermondynamisches Messen des Gesamtwirkungsgrades and hydrostatischen Antrieben“, *O + P : Zeitschrift für Fluidtechnik*, S. 285–287, 1973.
[40] W. Uffrecht, B. Heinschke, A. Günther, V. Caspary, und S. Odenbach, „Measurement of heat transfer coefficients at up to 25,500g - A sensor test at a rotating free disk with complex telemetric instrumentation“, *International Journal of Thermal Sciences*, Bd. 96, S. 331–344, 2015, doi: 10.1016/j.ijthermalsci.2015.03.006.
[41] J. Li, Ying, Xu, Bing, Zhang, „Experimental study on churning losses reduction for axial piston pumps“, in *IFK2018*, 2018.